Princeton Plasma Physics Laboratory

PPPL- 4880

PPPL- 4880

Dependence of the L-H Transition on X-point Geometry and Divertor Recycling on NSTX

D.J. Battaglia et. al.

May, 2013

PPPL PRINCETON PLASMA PHYSICS LABORATORY

Prepared for the U.S. Department of Energy under Contract DE-AC02-09CH11466.

Princeton Plasma Physics Laboratory
Report Disclaimers

Full Legal Disclaimer

Trademark Disclaimer

PPPL Report Availability

Princeton Plasma Physics Laboratory:

http://www.pppl.gov/techreports.cfm

Office of Scientific and Technical Information (OSTI):

http://www.osti.gov/bridge

Related Links:

U.S. Department of Energy

Office of Scientific and Technical Information

Fusion Links

Dependence of the L-H Transition on X-point Geometry and Divertor Recycling on NSTX

D.J. Battaglia[1], C.S. Chang[1], S.M. Kaye[1], K. Kim[2], S. Ku[1], R. Maingi[3], R.E. Bell[1], A. Diallo[1], S. Gerhardt[1], B.P. LeBlanc[1], J. Menard[1], M. Podesta[1], and the NSTX Team

[1] *Princeton Plasma Physics Laboratory, Princeton, NJ, USA*
[2] *Korea Advanced Institute of Science and Technology, Daejoen, Korea*
[3] *Oak Ridge National Laboratory, Oak Ridge, TN, USA*

E-mail contact of main author: dbattagl@pppl.gov

Abstract The edge electron (T_e) and ion temperature (T_i) at the time of the L-H transition increase when the X-point radius (R_X) is reduced to a high-triangularity shape while maintaining constant edge density. Consequently the L-H power threshold (P_{LH}) is larger for the high-triangularity shape. This supports the prediction that a single-particle loss hole, whose properties are strongly linked to R_X and T_i, influences the edge radial electric field (E_r) and $E_r \times B$ flow-shearing rate available for turbulence suppression. Simulations using XGC0, a full-f drift-kinetic neoclassical code, indicate that maintaining a constant $E_r \times B$ flow-shearing rate does require a larger heat flux and edge T_i as R_X decreases. NSTX also observes a decrease in P_{LH} when the divertor recycling is decreased using lithium coatings. However, the edge T_e and T_i at the L-H transition appear independent of the divertor recycling for a constant shape. XGC0 calculations demonstrate that more heat flux is needed to maintain the edge T_i and the $E_r \times B$ flow-shearing rate as the contribution of divertor recycling to the overall neutral fueling rate increases.

1. Introduction

The H-mode regime [1] is an attractive operating scenario for future magnetic confinement fusion devices, such as ITER [2]. This regime features a broad core pressure profile leading to improved magneto-hydrodynamic (MHD) stability, and a large edge pressure gradient that allows the plasma temperature in contact with the wall to be low while the core temperature is high. The bifurcation of the plasma confinement from an initial low confinement state (L-mode) to H-mode is attributed to an abrupt reduction in the turbulence-driven transport near the plasma edge [3]. This localized reduction in energy and particle transport leads to the formation of an H-mode pedestal with a steep gradient in the radial pressure profile.

The turbulence suppression mechanism of H-mode remains under investigation, but there is strong evidence that $E_r \times B$ flow shear plays the key role via the decorrelation of turbulence and the stabilization of microinstabilities that drive turbulence [4]. The amplitude of the cross-field flow shear can have a number of sources, including a mean component driven by the global plasma equilibrium, oscillating components such as the field from turbulence driven zonal flows [5], and small transient contributions emanating from core instabilities. Recent work has leveraged high-resolution edge diagnostics to examine the connection between $E_r \times B$ flow shear, local plasma parameters and the nature of the L-H transition [6,7]. Generally it is found that two conditions must be met to achieve H-mode: a transient reduction in the turbulent energy (L-H trigger) involving the oscillating or transient fields, and sufficient mean flow shear to sustain the turbulence suppression through the development of an edge pedestal. If the conditions for the trigger mechanism are achieved and sufficient mean flow shear is not

established, the turbulence is suppressed only briefly and the plasma state returns to L-mode. In cases where a limit-cycle oscillation occurs between L- and H-mode [8] it is observed that the plasma only enters a stationary H-mode once the mean flow shear that develops through the limit-cycle reaches a critical value [9].

Predicting and controlling the L-H transition is important for the design and operation of future tokamak reactors. In tandem with the development of first-principles models, resources have been directed toward identifying the experimental conditions required for initiating the L-H transition. One common metric is the minimum power conducted through the plasma boundary at the time of the threshold, i.e. the L-H power threshold or P_{LH}. Analysis of P_{LH} values from tokamaks satisfying ITER-relevant parameters for deuterium plasmas gives an empirical scaling for P_{LH} [10]

$$P_{LH\ ITER} = 0.0488 e^{\pm 0.057} n_e^{0.717 \pm 0.035} B_T^{0.803 \pm 0.032} S^{0.941 \pm 0.019} \qquad (1)$$

where n_e is the line-averaged electron density (10^{20} m^{-3}), B_T is the on-axis toroidal field (T) and S is the plasma surface area (m^2). This scaling relationship indicates that initiating the L-H transition requires larger heat flux though the plasma boundary (P_{LH}/S) as the global electron density and toroidal field increase. Expanding the P_{LH} dataset to include discharges outside the ITER-relevant parameter ranges reveals a multitude of additional dependences. This includes a strong dependence on the ion grad-B drift direction, a non-monotonic dependence on the global density, and larger values for low aspect ratio geometries. This article investigates two other well-documented dependences: the nature of the neutral fueling and X-point radial location.

The neutral fueling in L-mode is provided by wall sources (recycling, outgassing, sputtering, etc.) and active sources (gas puffing, neutral beams, pellet fueling, etc.). The properties of the neutral fueling sources, such as the poloidal location and fueling efficiency, can impact P_{LH} independent of any changes to the global or edge plasma density. For example, P_{LH} is often observed to be lower when gas fueling is injected from the inboard (high-field) as opposed to the outboard (low-field) side [11]. Also, the P_{LH} typically decreases as the fueling efficiency is increased, which can be altered by changing the active fueling source or the distance between recycling surfaces and the plasma edge. Typically, neutral fueling from divertor recycling is a significant fraction of the fueling source in diverted L-mode discharges.

One method for altering the nature of divertor recycling is by changing the geometry of the plasma X-point and strike-points in the divertor. Therefore, it is expected that moving the X-point radially will alter the neutral fueling characteristics and could possibly describe any impact the X-point movement has on P_{LH}. However, altering the X-point radius (R_X) has been hypothesized to impact P_{LH} through other mechanisms as well. The ambipolar E_r near the separatrix set by neoclassical ion transport is sensitive to R_X due to an ion orbit loss hole. This modification of the traditional neoclassical transport by a loss hole in velocity space (i.e., X-transport) will be described in more detail in later sections. The poloidal distribution and, to a lesser extent, the flux-surfaced-averaged E_r is also expected to change with the X-point location due to a modification of the Pfirsh-Schluter equilibrium currents [12]. Changing R_X will also change the edge magnetic helicity and magnetic shear, which will alter the turbulence driven

sheared flows and the conditions for the L-H trigger [13]. Incidentally, these geometrical effects all predict that increasing R_X (i.e., decreasing triangularity) should lower the P_{LH}/S necessary for the L-H transition in the favorable grad-B geometry. However, some experiments from JET observe the opposite trend, which is proposed to result from changes in divertor recycling through a coupled reduction in Z_X dominating any geometrical effects [14].

The importance of the ion orbit loss hole and neutral fueling on the mean $E_r \times B$ shearing rate and the L-H transition has been considered for several decades [15]. The results presented in this article advance this research by demonstrating that large-scale numerical calculations of kinetic ion and neutral transport in the plasma edge quantitatively match an experiment performed on the National Spherical Torus Experiment (NSTX). The experiment, described in Section 2, examines the nature of the L-H transition in two extremes of X-point radius (R_X) over the wide range of fueling and divertor recycling regimes enabled by lithium wall conditioning. The significant experimental observation is that the edge ion and electron temperatures at the time of the L-H transition depend on R_X, but are fairly insensitive to changes in divertor recycling. This suggests there is no universal critical edge temperature for the L-H transition when considering different magnetic topologies. In Section 3, predictions derived from the X-transport theory [16] are shown to be consistent with the experimental observations. A full-f drift-kinetic neoclassical simulation code (XGC0) that captures the important X-transport and neutral fueling physics is shown to reproduce the experimental observation that the edge ion temperature required to generate a nominal level of $E_r \times B$ flow shear depends on R_X, but is insensitive to divertor recycling. However, the heat flux, and thus P_{LH}, needed to generate the required $E_r \times B$ flow shear depends on the nature of the neutral fueling. This agreement between experiment and the model suggests that X-transport and divertor recycling play a role in L-mode transport and should be included in first-principles models of the L-H transition.

2. Experiment on NSTX

NSTX is a low-aspect-ratio (R/a = 0.85/0.65 m ~ 1.3) device that routinely operates in H-mode with up to 7 MW neutral beam heating and 4 MW of high harmonic fast wave (HHFW). The L-H power threshold follows the scaling with n_e, B_T and S as Eq. 1, however the leading coefficient is typically two to ten times larger. NSTX has an open divertor and active control over the X-point position. A novel lithium evaporation system deposits thin (~ 10 nm) solid lithium coatings between shots to entrain impurities and provide continuous deuterium pumping during the discharge. This wall-conditioning system allows for shot-to-shot variations in the pumping rate, and can pump both legs of the divertor regardless of their strikepoint positions. The open divertor and flexible divertor pumping provide an opportunity to decouple the impact of R_X and divertor recycling on the L-H transition.

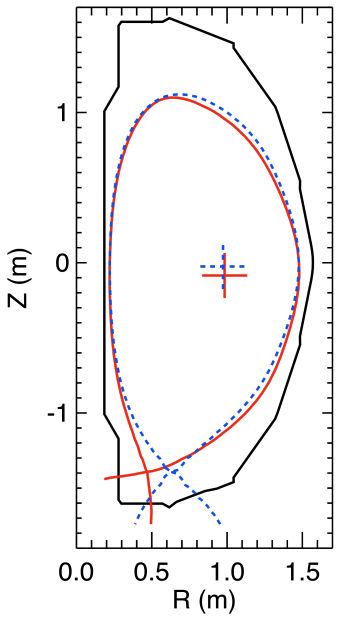

FIG. 1. Plasma separatrix for small-R_X (solid red) and large-R_X (dotted blue) shapes. Crosses indicate position of magnetic axis.

Data from the first experiments at NSTX to demonstrate the dependence of L-H transition on R_X are presented in [17], however the analysis was complicated by large variations in dW/dt and P_{OH} where dW/dt is the change in the plasma stored energy and P_{OH} is the resistive heating power. The new data reported in this paper remove that uncertainty by delaying the L-H transition to a time in the discharge with nearly stationary dW/dt and P_{OH}, and repeating the experiment over a range of divertor recycling conditions. Preliminary analysis of the present dataset is presented in recent overview papers [18].

The magnetic boundaries of the two discharges used in the experiment are shown in Fig 1. The boundaries are computed using an equilibrium reconstruction derived from magnetic data and an isothermal T_e constraint at the midplane [19]. One discharge has $R_X = 0.66$m ($\delta = 0.36$) while the other discharge has $R_X = 0.49$m ($\delta = 0.47$) where δ is the triangularity, $\delta = \left(R_0 + R_X\right)/\left(R_0 + r\right)$. The discharges have matched plasma current ($I_P = 0.8$ MA) and on-axis toroidal field ($B_{T0} = 0.54$ T) in the favorable ∇B configuration (ion grad-B drift is down). The discharges also have nearly matched X-point height, plasma surface area (29 m^2), and boundary locations at the midplane. The two discharge shapes were reproduced under three divertor recycling and neutral fueling conditions: (1) low divertor recycling and large inboard neutral gas fueling rate, (2) high divertor recycling and low inboard neutral gas fueling rate and (3) high divertor recycling and medium inboard neutral gas fueling rate. The low recycling divertor is achieved on NSTX by evaporating 300 mg of lithium on the divertor surfaces, while the high recycling divertor has passivated lithium coatings.

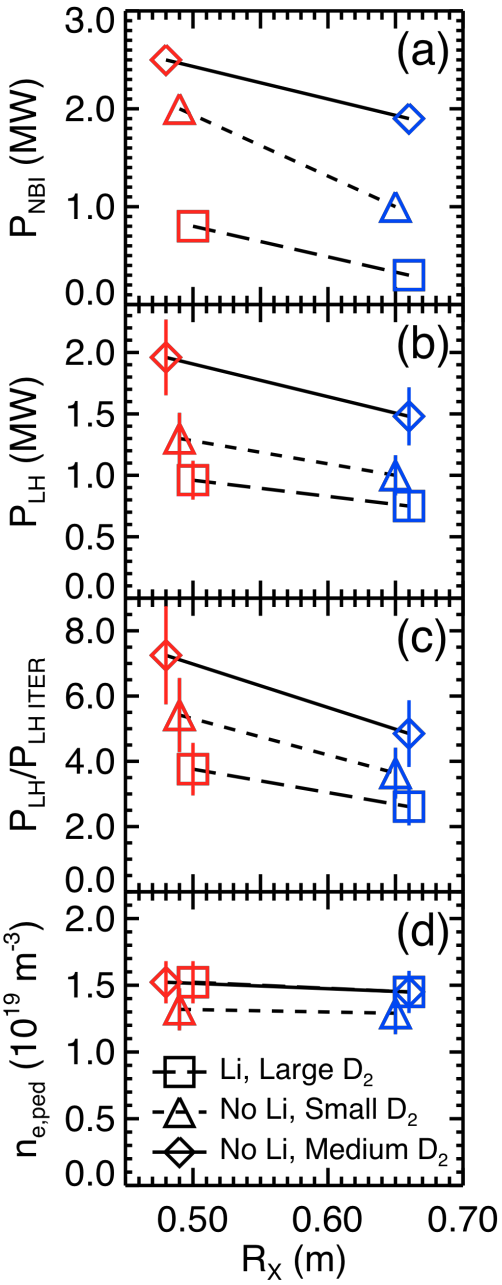

FIG. 2. (a) Minimum NBI power and (b) P_{LH} required for L-H transition for two different shapes in three different fueling conditions. (c) P_{LH} normalized to the ITER P_{LH} scaling and (d) the L-mode density pedestal height.

All of the discharges in this dataset establish a stationary 20 – 30 ms ohmically heated L-mode before adding neutral beam injection (NBI). P_{LH} was identified for each condition by running a series of discharges with incrementally larger NBI power until a long (> 30 ms) H-mode was observed no earlier than 50 ms (a few fast ion slowing down times) after the start of the NBI. At heating powers below P_{LH}, the discharges would often

dither (undergo frequent L-H-L transitions), but not achieve a long H-mode, suggesting the requirements for the L-H trigger were satisfied without the necessary mean $E_r \times B$ flow shear to sustain the H-mode.

The minimum NBI power (P_{NBI}) needed to access long H-modes for each shape in three different fueling scenarios is shown in Fig 2a. Lines are drawn to connect the data taken in matched neutral fueling cases and do not imply a linear trend. P_{NBI} is the lowest for the low recycling divertor (squares) for both shapes. The other two scenarios have a higher recycling divertor and the discharges with the lower neutral fueling rate (triangles) have a smaller P_{NBI} than the discharges with the larger neutral fueling rate (diamonds). The small-R_X (high δ) shape requires more neutral beam heating power to achieve H-mode than the large-R_X shape in each fueling scenario.

The loss power at the L-H transition ($P_{LH} = P_{heat} + P_{OH} - dW/dt$) is calculated using TRANSP analyses (Fig 2b). P_{LH} for the small-R_X shape is about 30% larger for each fueling scenario. The error in P_{LH} is approximated to be 15%, with a majority of the uncertainty due to systematic error in calculating the beam heating efficiency. Previous experiments [17] established that P_{LH} is approximately proportional to the line-averaged density (n_{el}), similar to the ITER scaling relationship (Eq 1). The large-R_X shape had a slightly larger line-averaged density than the small-R_X shape in all three fueling scenarios, which goes in the opposite direction of the change to P_{LH} with R_X. Figure 2c shows P_{LH} normalized to $P_{LH\,ITER}$, where the difference between the small-R_X and large-R_X shape is now about 46% for all three fueling scenarios.

The electron density (n_e) and temperature (T_e) profiles at the midplane are measured using a Multi-pulse Thomson Scattering system. The L-mode profiles are slowly evolving (both n_e and T_e are increasing < 10% between samples taken every 17 ms). The n_e profile has a pedestal that can be fit with a hyperbolic tangent function. The height of the n_e pedestal for the last L-mode profile is shown in Fig 2d. The first two fueling scenarios (squares and triangles) have similar L-mode line-averaged n_e but different pedestal densities. In this comparison, the strong pumping from lithium coatings decreased P_{LH} by about 20%. The third fueling scenario (diamonds) was operated at a higher line-averaged density, but matches the

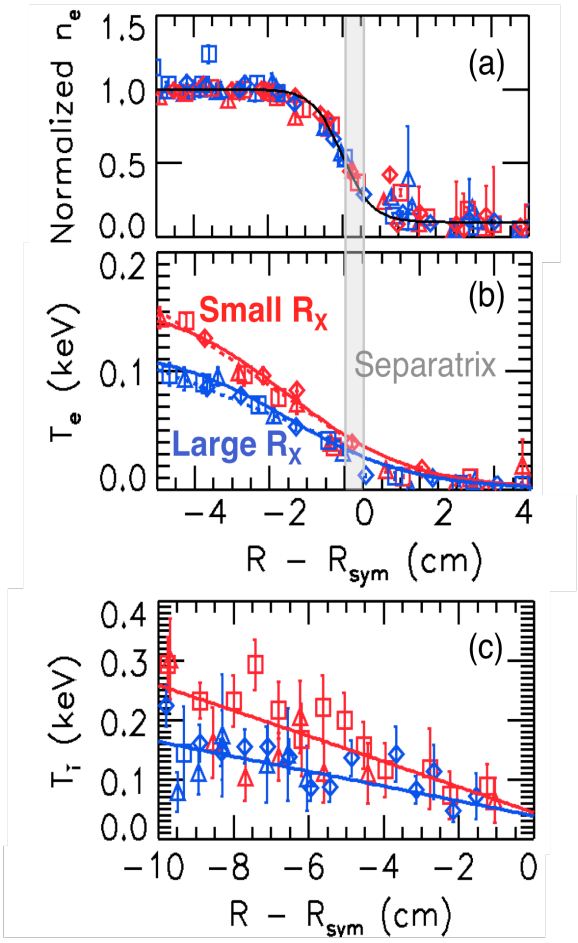

FIG. 3. (a) n_e / n_{eped}, (b) T_e, and (c) T_i near the time of the L-H transition for the six discharges

pedestal density of the low recycling divertor (squares). In this comparison, reduced recycling from lithium coatings leads to a near halving of P_{LH}.

Figure 3 shows a number of L-mode profiles preceding (within 17 ms) the L-H transition from the six discharges where the symbols and colors match Fig 2. In Fig 3a, n_e profiles are normalized to the pedestal height and aligned relative to the pedestal symmetry point. The gray vertical box indicates a typical range of the radial location of the separatrix based on power balance considerations [20]. The hyperbolic tangent fit for the data has a width of 1.5cm ($\Delta\psi_N \sim 0.045$). Figure 3b shows the T_e profiles for the same six discharges. The solid lines are hyperbolic tangent fits to the composite of the three profiles for each shape while the dotted lines are the linear fits to the T_i measurements described later. For a given shape (red or blue points), the edge T_e profile is similar despite a large range in the NBI heating and divertor recycling. However, the edge temperature does depend on R_X, as the T_e at the top of the density pedestal (–2 cm) is 30% larger for the small-R_X shape (red points) than the large-R_X shape (blue points). This is consistent with the 30% difference in heat flux (P_{LH}/S) for the two different shapes.

A direct measurement of the L-mode edge ion temperature (T_i) using passive and active CVI charge-exchange spectroscopy measurements is hindered by poor carbon confinement in L-mode. Figure 3c shows the active CVI measurements with least squares linear fit of the data for each experimental shape. The linear fits are also over-plotted on Fig 3b as dotted lines. While the measurements were insufficient to constrain the local T_i in the edge region, the extrapolated core measurements suggest $T_i \sim T_e$ up to the top of the density pedestal (– 2 cm). This assumption is reasonable considering that the thermal equilibration of the main ions and electrons is on the order of a few milliseconds when $T_e \sim 100$ eV [21], which is several times shorter than the local electron thermal confinement time at the top of the density pedestal for typical L-mode NSTX discharges.

The following conclusions are derived from these data: (1) P_{LH} increases with the larger divertor recycling and smaller R_X, and (2) the edge T_e ($\sim T_i$) near the time of the L-H transition is independent of the divertor pumping and fueling conditions, but increases as R_X decreases to a high triangularity shape. The observation of a consistent edge temperature at the L-H transition that depends on R_X supports the predictions of X-transport theory, as described in the next section.

3. Full-f Neoclassical Ion Transport Calculations

X-transport theory predicts that thermal ion orbit loss around the X-point can lead to neoclassical plasma transport that is not automatically ambipolar. This source of non-ambipolar transport impacts E_r near the plasma boundary and is a function of R_X [22,23]. The impact of R_X on the loss hole is illustrated here using a single particle guiding center model in the absence of any electric fields, collisions or flows (single-particle orbit calculation in XGC0 is described in [24-25]). In these conditions, the lowest energy loss orbits are counter-I_p trapped ions that originate from the outboard midplane ($R > R_0$ and $d\psi/dz = 0$) and are lost to the inner divertor leg when $\nabla B \times B$ is pointing toward the X-point (favorable ∇B configuration). Higher energy counter-I_p ions on passing orbits can be lost to the outer divertor leg. The velocity space loss hole in pitch-energy space for ions launched at $\psi_N = 0.96$ ($\Delta r = -1.3$ cm from separatrix) at the

outboard midplane of the two NSTX shapes are shown in Fig 4. The position of the launch location (Δr) along the midplane is near the top of the pedestal region; however, the launch depth is arbitrary in this model since the energy axis scales approximately as Δr^2 [22]. Counter going ions launched with pitch (= $v_{||}/v$) and energy components in the unshaded region are either confined passing or trapped orbits (regions labeled P and T, respectively). The loss hole (shaded region) is divided into two regions: the lower-energy ions lost to the inner (I) divertor leg and the higher-energy ions lost to the outer (O) divertor leg.

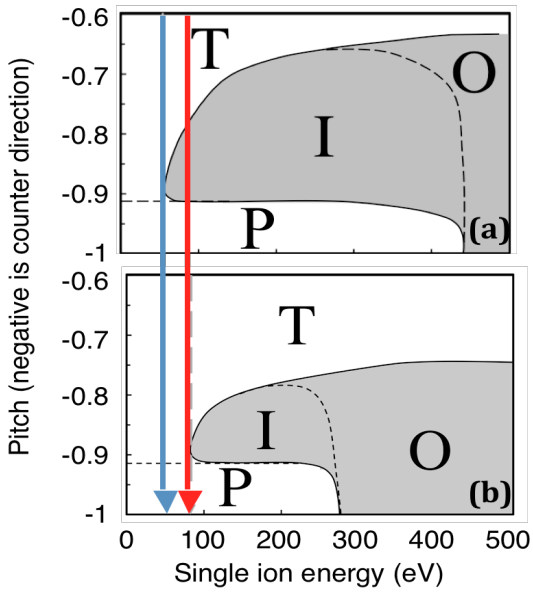

FIG. 4. Ion velocity loss hole at $\Psi_N = 0.96$ on the outboard midplane for (a) large-R_X shape and (b) small-R_X shape. Arrows indicate critical loss energy. Note suppressed vertical axes.

The vertical arrows in Fig 4 indicate the minimum unconfined ion energy (K_0) for the two different plasma shapes. The K_0 for the large-R_X shape is 71 eV (Fig 4a and blue arrow), while the K_0 for the small-R_X shape is 96 eV (Fig 4b and red arrow), which is 35% larger. The reduction in K_0 with increasing R_X is due to (1) longer ion bounce orbits prior to entering the X-point region and (2) lower B_Z shear in the X-point region. The large-R_X shape also has a larger loss region above K_0 compared to the small-R_X shape since more trapped orbits have bounce points inboard of the X-point. The relative differences in the loss holes, including the 35% difference in K_0, are the same for all points along the midplane in the edge region ($\psi_N > 0.85$).

The change in the loss holes with R_X is consistent with the observed dependence of the L-H transition on R_X. Under matched densities and temperatures, more ions in a Maxwellian distribution would reside in the loss hole for the low triangularity shape (Fig 4a) and would require a more negative E_r to close the loss hole enough to maintain ambipolar transport. This leads to a larger degree of $E_r \times B$ flow shear, which is favorable for the L-H transition. One way to match the $E_r \times B$ flow shear for the two shapes is to increase edge T_i for the high-triangularity shape. The larger T_i enhances X-transport by increasing the number of loss orbits in the loss hole and increases the edge pressure gradient. Both effects conspire to drive the neoclassical E_r more negative and enhance the flow shear.

This argument is quantitatively illustrated using the full-f XGC0 code [25], which solves the single particle drift-kinetic equations for about ten million test ions in the magnetic fields from an MHD equilibrium solution (see Fig 1). The ion particles are initially distributed throughout a 5D space (3D volume, 2D velocity) assuming Maxwellian distributions based on experimental measurements of T_i, n_i, and toroidal velocity at the midplane. The position and energy of the particles is advanced in discrete timesteps (~ 100 ns) assuming Monte-Carlo

collisions with a Maxwellian background (linear collision operator). E_r is adjusted self-consistently to maintain ambipolar transport across flux surfaces. Any particle that is lost to a wall is reborn as a neutral atom particle at the wall with a random launch direction. A Monte-Carlo random-walk model is used to follow the neutral trajectory until it is ionized. The local plasma parameters are calculated and compared to experiment by taking moments of the distribution function derived from the thousands of test ions found within a localized R,Z range.

The model has three free input parameters that are chosen such that ion temperature, density and rotation profiles at the outboard midplane remain stationary (over a few milliseconds) and closely match the experimental measurements. Heat and toroidal torque are applied at the core boundary of the simulation ($\psi_N = 0.85$), which accounts for the transport of

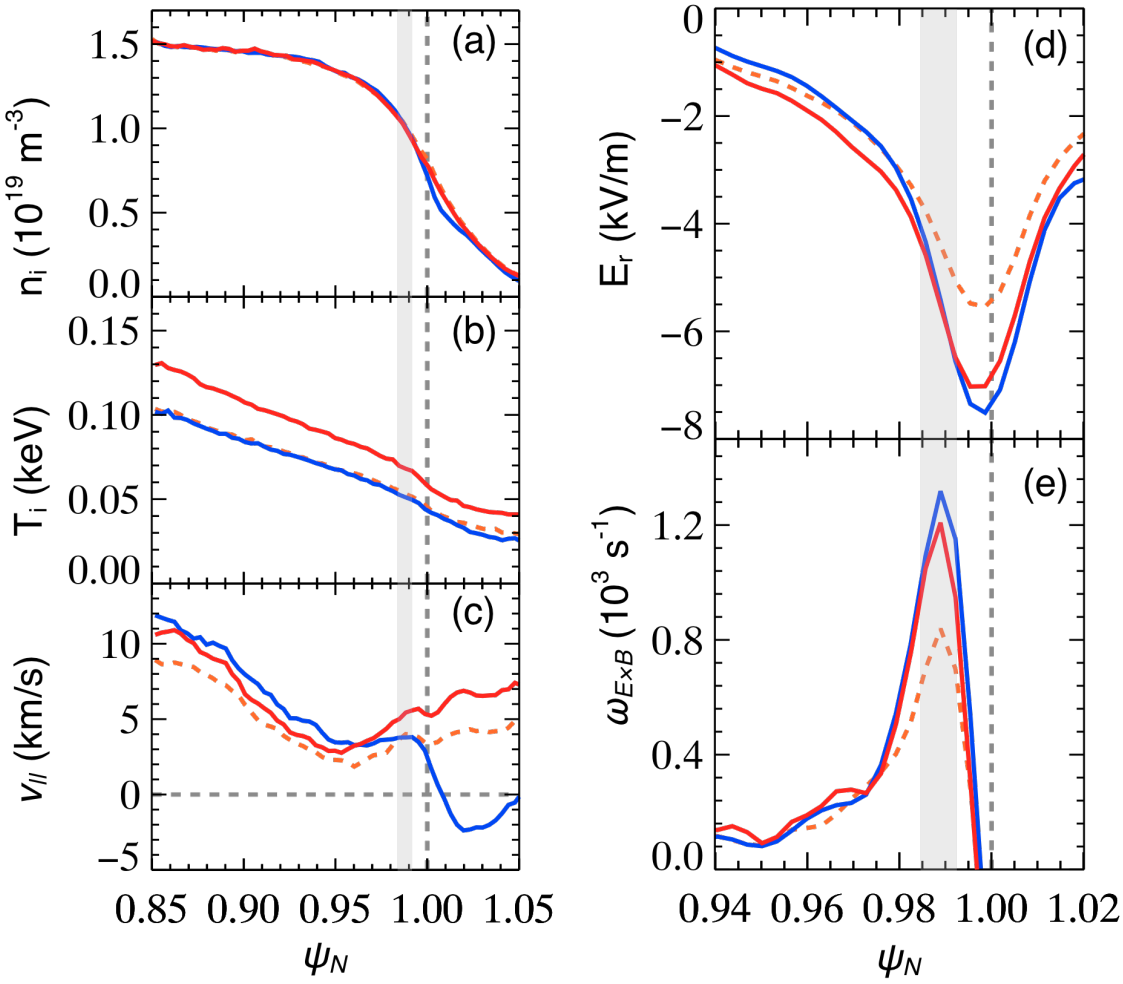

FIG 5. XGC0 calculated flux-surface-averaged (a) n_i, (b) T_i and (c) parallel flow for the large-R_X shape (solid blue) and the small-R_X shape (dotted orange) with matched core heating and torque. The small-R_X shape with core heating and torque increased by 30% (solid red) provides a good match to the midplane (d) E_r and (e) shearing rate of the large-R_X case in the shaded region.

NBI energy deposited in the core. The third free parameter is a random walk particle diffusion step-size that is added as a proxy for ambipolar particle diffusion from turbulent transport. In all simulations, the step-size equates to an anomalous particle and energy diffusion of 0.1 m^2/s across the entire midplane. Without this added transport, the simulated profile gradients become steeper than the measured L-mode profiles.

The calculated equilibrium n_i (more correctly, the guiding center density $n_{i,gc}$), T_i and ion $v_{//}$ profiles (co-I_p is positive) are shown in Fig. 5. The blue and dotted orange lines show the simulation results for the large-R_X and small-R_X shapes where core heating and torque are matched. The solid red traces are the results for the small-R_X shape where the core heating and torque were increased by 30%, resulting in larger temperatures and parallel flows for the same density.

The corresponding E_r and Hahm-Burrell $E_r \times B$ shearing rate [26] at the outboard midplane are shown in Fig. 5 (c-d). The shaded region indicates the position of maximum shear rate. The important observation is that the large-R_X shape (blue) has a deeper E_r well than the small-R_X simulation with matched conditions (dotted orange) due to the enhanced X-transport. Consequently, the $E_r \times B$ shear rate achieves a larger peak for the large-R_X shape. When the core heating and torque flux are increased by 30% for the small-R_X shape (solid red), the E_r well becomes deeper and the peak shear rate nearly matches the lower power large-R_X shape. Therefore, if establishing a long H-mode state requires a critical $E_r \times B$ shear rate that is independent of R_X, then the simulation results support the experimental observation that both the core heating and edge temperature must be 30% larger for the small R_X (high triangularity) shape.

The equilibrium parallel energy distribution for ions inside a toroidal ring at the outboard midplane (Fig. 6) illustrates the impact of the ion velocity loss hole. E_r is driven negative until the confinement of high-energy ions is improved such that the loss of counter-I_p ions is balanced by a pinch of co-I_p ions. The resulting shift of the Maxwellian at high energies is transferred to the bulk ions through collisions, generating an "intrinsic" torque in the co-I_p direction [27]. The resulting co-I_p flow layer accounts for the small bump in the flow profiles for $0.95 < \psi_N < 1$ in Fig 5c. The distributions look similar for both shapes with matched conditions, but it takes a more negative E_r to achieve the ambipolar balance with large R_X.

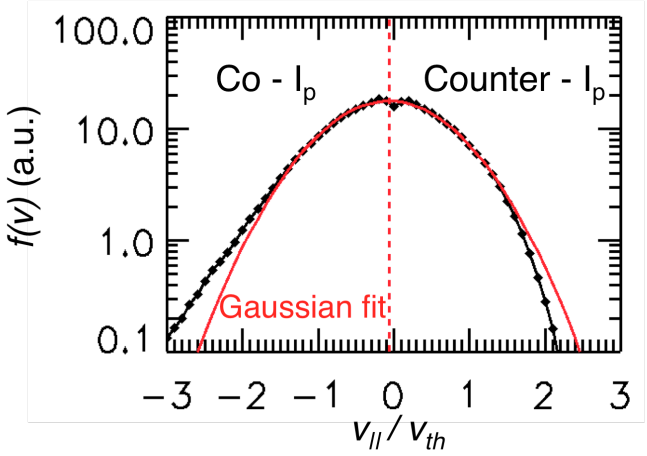

FIG. 6. (Black) Calculated $v_{//}/v_{th}$ test particle distribution in a toroidal ring: $0.985 < \psi_N < 0.995$ and $-10° < \theta < 10°$. (Red) Gaussian fit of distribution. Dotted red line shows center of Gaussian shifted toward co-I_p.

The impact of divertor recycling on P_{LH} is investigated with XGC0 by comparing two different recycling models

in the code. The results shown in Fig 5 use a model where a neutral particle is born from the location where it was lost to the wall. This is typical of a high recycling divertor where most of the neutral fueling comes from divertor recycling. To simulate a lower recycling divertor, a lost ion is reborn as a neutral in a random poloidal position on the wall. Consequently the neutral density is more evenly distributed poloidally around the plasma. This type of calculation is used as a proxy for a low recycling divertor with a gas puff in the upper chamber that is supplying a portion of the fueling. A detailed comparison of these two recycling models is reported in [28].

The results from the two models are summarized in Fig 7. The blue traces are repeated from Fig 5, while the black profiles are for the same shape with the low recycling divertor model. Distributing the neutral density throughout the SOL improves the fueling efficiency, reducing the loss of energy and momentum to charge-exchange in the SOL. Consequently, the core heating and torque are reduced by 36% in order to maintain a similar T_i (Fig 7b), parallel flow velocity (Fig 7c) and $E_r \times B$ flow shearing rate (Fig 7e). The low-recycling divertor model

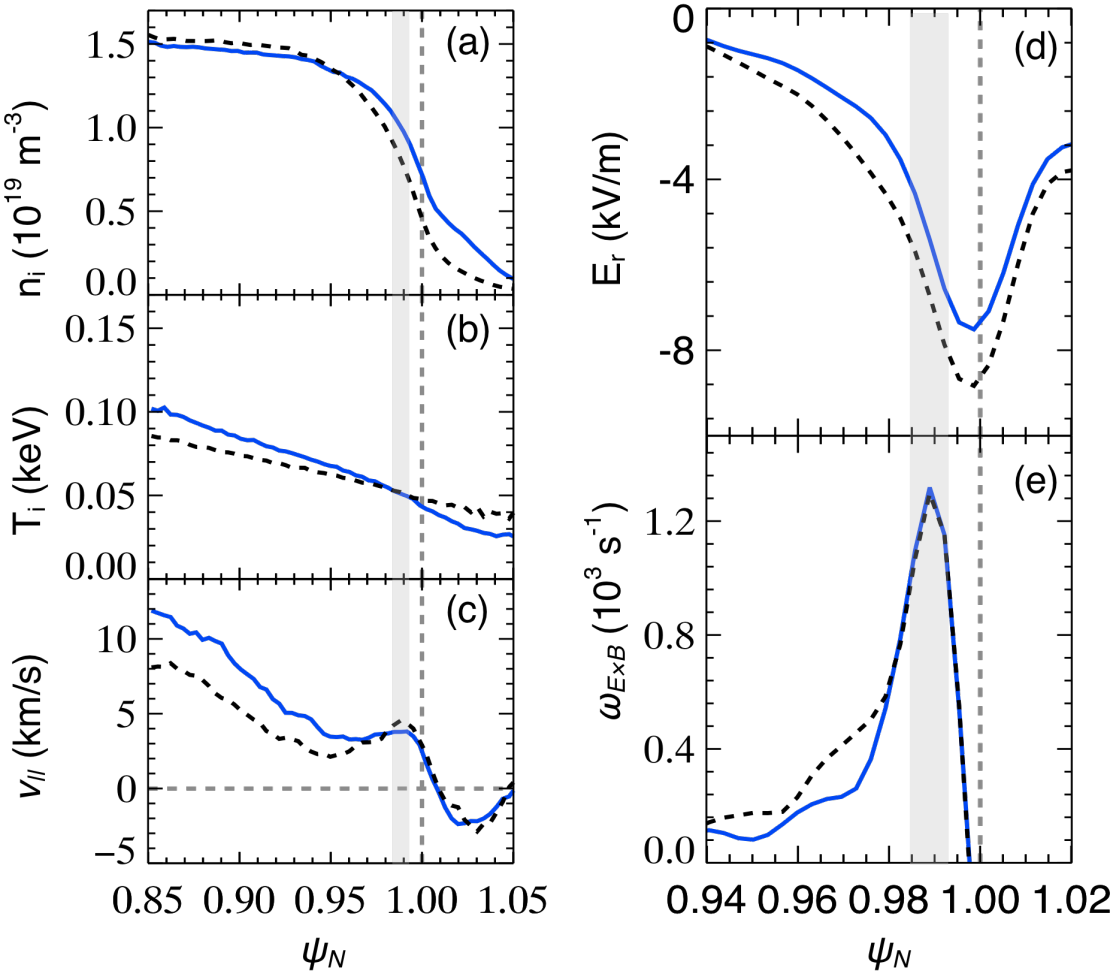

FIG 7. XGC0 calculation with high-recycling (solid blue) and low-recycling (dashed black) divertor model. The low-recycling simulation has the core heating and torque reduced by 36% to provide a good match to (e) the edge $E_r \times B$ flow shearing rate.

leads to a density profile that is shifted inward with a lower SOL density. This is consistent with H-mode experiments on NSTX that observe the density pedestal symmetry point moves inward as the divertor recycling is reduced using lithium coatings [29].

The experimental results found a nearly 50% reduction in P_{LH} when lithium was used to reduce the divertor recycling while maintaining a constant pedestal density height. Therefore, the 36% reduction in the simulation achieves the correct trend, but under predicts the experimental result. A more localized inboard gas puff model may improve the quantitative match; this capability exists in XGC0, but is not used in the present study.

The presented XGC0 calculations make some assumptions that are not completely self-consistent. For example, the electron and impurity profiles are held constant (only main ion transport is evolved), no kinetic electron effects are considered and the collision operator is linear. Furthermore, the magnetic topology and anomalous transport rates remain fixed in time and space. The XGC0 and XGC1 suite of codes are capable of evolving these fixed parameters for a more self-consistent solution at the cost of larger calculations. It is anticipated that expanding the presented calculations would change the magnitude of E_r and the flow shear, but the relative impact of R_X and T_i on E_r near the separatrix would remain.

4. Conclusion

This paper presents experimental and computational evidence that the required edge ion temperature for sustaining the H-mode after the L-H transition trigger varies with the X-point radius. This observation is in agreement with the prediction from kinetic neoclassical theory that the mean $E_r \times B$ flow shear required to sustain the H-mode depends on the edge E_r required to close the ion orbit loss hole and maintain ambipolar transport across flux surfaces and the separatrix. Single-particle orbit calculations (absent of E_r and collisions) illustrate the dependence of the critical energy of the ion orbit loss hole with R_X. Full-f drift-kinetic XGC0 simulations with self-consistent collisions and neutral recycling are in quantitative agreement with NSTX experiments that found the E_r x B flow shear rate is matched when the edge T_e ($\sim T_i$) at L-H transition is 30% larger as R_X was moved 17 cm inward.

The edge temperature at the L-H transition was observed to depend on R_X, but not the neutral fueling conditions despite the fact that the heat flux (P_{LH}/S) through the edge varied strongly with the divertor recycling and midplane fueling rates. The interpretation drawn from the kinetic neutral fueling model in XGC0 is that the neutral fueling efficiency (confined particles per ionizations) is smaller when the fueling is provided primarily from the divertor as opposed to the main chamber. Thus, a larger SOL neutral density is required to maintain the L-mode density, which removes more energy through charge-exchange and ionization from the edge plasma. In other words, a high-recycling divertor requires a larger heat flux to raise the edge temperature up to the critical value for the L-H transition compared to a low-recycling condition. This translates into a variation of P_{LH} with the neutral fueling conditions that is independent of the critical edge T_i.

The variation of the edge temperature with R_X can translate into a change in P_{LH} since a larger edge temperature requires an increase in the heat flux through the edge. However, the relationship between the edge T_i and heat flux is typically dominated by the ion-neutral physics and could dictate the impact of R_X on P_{LH}. NSTX has an open divertor and the ability to pump both divertor legs using lithium coatings independent of the strike points. This minimizes the variation in neutral recycling with changes in R_X, and thus P_{LH} was observed to follow the 30% change in edge T_i with R_X. It is important to recognize that this may not be the case in other tokamaks, where the recycling will vary with R_X due to a closed divertor and/or poloidally localized pumps. Therefore, P_{LH} could increase when going to lower triangularity with a smaller critical T_i if the neutral density is concurrently increasing. Furthermore, the kinetic effects and the critical L-mode T_i are sensitive to other shaping parameters (such as R_{in}, R_{out}, and elongation) that are not often matched when altering R_X due to constraints on plasma control.

The data and modeling presented in this paper lends strong support for the theory that an ion velocity loss hole influences the edge E_r in L-mode and thus the $E_r \times B$ flow shear available to sustain the H-mode following the L-H transition trigger. Therefore, the edge ion temperature at the time of the L-H transition is not universal and will depend on the critical energy of the loss hole. The ion orbits that set the critical energy of the ion velocity loss hole occur close to the trapped-passing boundary, therefore the variation of the edge T_i with R_X is expected in all tokamaks regardless of aspect ratio. A testable hypothesis that can be extended to other tokamak experiments is the prediction that the L-H transition requires a critical L-mode edge T_i that depends on the magnetic geometry, but does not vary strongly with the neutral fueling conditions or edge density. This hypothesis is predicated on the assumption that the critical E_r and $E_r \times B$ flow shear rate for establishing H-mode does not vary with experimental parameters, which requires further study of the multi-scale interaction of turbulence and flows.

Looking ahead, the predictions of X-transport can be exploited to reduce the heating power demands of future tokamaks. For example, a discharge could start with a large R_X to facilitate H-mode access at lower heating power, and then shift R_X to smaller values while in H-mode to optimize MHD stability and the achievable density relative to the Greenwald density limit scaling. Also, the role of the edge T_i in establishing the necessary $E_r \times B$ flow shear for sustaining the L-H transition highlights the importance of controlling divertor recycling in order to optimize the fueling efficiency. Future computational and experimental work will focus on quantifying the relationship between the E_r and the edge profiles, especially T_i, in light of the prediction that kinetic neoclassical transport is significant in the L-mode edge.

This work was funded by the US Department of Energy under Contract Numbers DE-AC02-09CH11466 and DE-AC05-00OR22725. This research used resources of the National Energy Research Scientific Computing Center, which is supported by the Office of Science of the U.S. Department of Energy under Contract No. DE-AC02-05CH11231.

[1] WAGNER, F., et al., *Phys. Rev. Lett.* **49** (1982) 1408-12

[2] SHIMADA, M., et al., Progress in the ITER Physics Basis Chapter 1: Overview and Summary 2007 *Nucl. Fusion*, **47** S1

[3] Connor, J., & Wilson, H. *PPCF*, **1** (1999), 0–74.
Wagner, F. *PPCF*, **49** (2007) B1–B33.

[4] BURELL, K.H., *Phys. Plasmas*, **4** (1997) 1499-518

[5] Diamond, P.H., Itoh, S.-I., Itoh, K., and Hahm, T.S. *PPCF* **47** (2005) R35
Fujisawa, A., *Nucl. Fusion* **49** (2009) 013001

[6] Sauter, P., Pütterich, T., Ryter, F., Viezzer, E., Wolfrum, E., Conway, G. D., Fischer, R., et al. *Nucl. Fusion*, ***52*** (2012) 012001.

[7] Manz, P., Xu, G. S., Wan, B. N., Wang, H. Q., Guo, H. Y., Cziegler, I., Fedorczak, N., et al. *Phys. Plasmas*, ***19*** (2012) 072311

[8] Kim, E., Diamond, P.H., *Phys. Rev. Lett.* **90**, (2003) 185006

[9] Schmitz, L. et al., *Phys. Rev. Lett.* **108** (2012) 155002

[10] MARTIN, Y.R., et al., *J. Physics: Conf. Series* **123** (2008) 012033

[11] Maingi, R., Chang, C. S., Ku, S., Biewer, T., Maqueda, R., Bell, M., Bell, R., et al. *PPCF*, ***46*** (2004) A305–A313

[12] Aydemir, A. Y. *Nuclear Fusion*, ***52*** (2012) 063026

[13] Fedorczak, N., Diamond, P. H., Tynan, G., & Manz, P. *Nucl. Fusion*, ***52*** (2012) 103013

[14] Andrew, Y., Hawkes, N., O'Mullane, M., & Sarori, R. *Phys. Plasmas **87*** (2004)

[15] Itoh, S., & Itoh, K. *Nucl. fusion*, **29** (1989) *1031*

[16] CHANG, C.S., et al., *Phys. Plasmas*, **9** (2002) 3884-92

[17] MAINGI, R., et al., *Nucl. Fusion* **50** (2010) 064010

[18] KAYE, S.M., et al., *Nucl. Fusion* **51** (2011) 113019
RAMAN, R., et al. *Nucl. Fusion* **51** (2011) 094011
HAWRYLUK, R.J., *Nucl. Fusion* **51** (2011) 094005

[19] MENARD, J.E., et al., *Phys. Rev. Lett.* **97** 095002

[20] Pitcher, C., & Stangeby, P. *PPCF*, **39** (1997) *779*

[21] NRL Plasma Formulary, NRL/PU/6790-02-450

[22] CHANKIN, A.V., and McCRAKEN, G.M., *Nucl. Fusion* **33** (1993) 1459-69

[23] MIYAMOTO, K., *Nucl. Fusion* **36** (1996) 927-38

[24] KU, S., et al., *Phys. Plasmas*, **11** (2004) 5626-33

[25] CHANG, C.S., et al, *Phys. Plasmas* **11** (2004) 2649-67

[26] Hahm, T. S., & Burrell, K. H. *Phys. Plasmas **2*** (1995), 1648

[27] DeGRASSIE, J.S. et al., *Nucl. Fusion* **52** (2012) 013010

[28] STOTLER, D.P. et al., *J. Nuclear Materials, in Press (2012)* http://dx.doi.org/10.1016/j.jnucmat.2013.01.046

[29] Maingi, R., Osborne, T., LeBlanc, B., Bell, R., Manickam, J., Snyder, P., Menard, J., et al. *Phys. Rev. Lett., 103* (2009), 075001

The Princeton Plasma Physics Laboratory is operated
by Princeton University under contract
with the U.S. Department of Energy.

Information Services
Princeton Plasma Physics Laboratory
P.O. Box 451
Princeton, NJ 08543

Phone: 609-243-2245
Fax: 609-243-2751
e-mail: pppl_info@pppl.gov
Internet Address: http://www.pppl.gov